Journal Pre-proofs

Temperature Cycling-Induced Formation of Crystalline Coatings

Sarah Zellnitz-Neugebauer, Magdalena Lanzinger, Hartmuth Schroettner, Majid Naderi, Meishan Guo, Amrit Paudel, Heidrun Gruber-Woelfler, Peter Neugebauer

PII: S0378-5173(22)01132-2
DOI: https://doi.org/10.1016/j.ijpharm.2022.122577
Reference: IJP 122577

To appear in: *International Journal of Pharmaceutics*

Received Date: 23 September 2022
Revised Date: 28 December 2022
Accepted Date: 29 December 2022

Please cite this article as: S. Zellnitz-Neugebauer, M. Lanzinger, H. Schroettner, M. Naderi, M. Guo, A. Paudel, H. Gruber-Woelfler, P. Neugebauer, Temperature Cycling-Induced Formation of Crystalline Coatings, *International Journal of Pharmaceutics* (2022), doi: https://doi.org/10.1016/j.ijpharm.2022.122577

Temperature Cycling-Induced Formation of Crystalline Coatings

Sarah Zellnitz-Neugebauer[1+], Magdalena Lanzinger[2], Hartmuth Schroettner[3,4], Majid Naderi[5], Meishan Guo[5], Amrit Paudel[1,2], Heidrun Gruber-Woelfler[1,2] and Peter Neugebauer[1,2+]*,

[1] *Research Center Pharmaceutical Engineering GmbH, Graz, 8010, Austria*

[2] *Institute of Process and Particle Engineering, Graz University of Technology, Graz, 8010, Austria*

[3] *Institute of Electron Microscopy and Nanoanalysis (FELMI), Graz University of Technology, Graz, 8010, Austria*

[4] *Graz Centre for Electron Microscopy (ZFE), Graz, 8010, Austria*

[5] *Surface Measurement Systems Ltd., London, HA0 4PE, United Kingdom*

+ Both authors contributed equally to this work

* Corresponding author: Peter Neugebauer, peter.neugebauer@tugraz.at, Tel: +43 316 873 30424

Abstract

The surface of particles is the hotspot of interaction with their environment and is therefore a major target for particle engineering. Particles with tailored coatings are greatly desired for a range of different applications. Amorphous coatings applied via film coating or microencapsulation have frequently been described in the pharmaceutical context and usually result in homogeneous surfaces. In the present study we have been exploring the feasibility of coating core particles with crystalline substances, a matter that has rarely been investigated. The expansion of the range of possible coating materials to include small organic molecules enables completely new product properties to be achieved. We present an approach based on temperature cycles performed in a tubular crystallizer to result in engineered crystalline coatings on excipient core particles. By manipulating the process settings and by the choice of coating substance we are able to tailor surface roughness, topography as well as surface chemistry.

Benefits of our approach are demonstrated by using resulting particles as carriers in dry-powder-inhaler formulations. Depending on the resulting surface chemistry and surface roughness, coated carrier particles show varying fitness for delivering the model API salbutamol sulphate to the lung.

KEY WORDS: coating crystallization, cross-nucleation, surface nucleation, heteroepitaxy, dry powder inhalation

1 INTRODUCTION

For coating tablets and granules, film coating is the most commonly used method to apply amorphous layers of polymers. In the pharmaceutical context, coatings can improve the stability of the core substance against destructive handling or storage conditions (light, oxygen, etc.), modulate drug release profiles, or simply improve drug taste and appearance (Gaur et al., 2014). In this respect, pharmaceutical development has equipped formulation experts with a toolbox of different coating polymers from which to choose. The homogeneity and uniformity of the resulting coating generally is regarded as a desired feature.

While there has been a focus on targets named above, other means of coatings have received less interest in the pharmaceutical context. The possibilities offered by small organic molecules to form of crystalline coatings and the prospects of heterogeneous surfaces with high surface roughness have hardly been exploited so far. Accordingly, only a very limited amount of respective literature is available and there is a lack of suitable manufacturing techniques (Kim and Ulrich, 2003a, 2003b; Römbach and Ulrich, 2007). Although high surface roughness is mostly undesirable for today's drug formulations, its targeted use offers new possibilities for future applications. The coating of particles by means of crystallization processes provides opportunities of applying a much wider range of substances. This increased flexibility in the selection of the coating substance ultimately offers the possibility of optimizing particles' surface chemistry according to their application.

Applying Crystalline Coatings

The formation of crystalline coatings is generally based on heterogeneous nucleation and heteroepitactic growth, i.e. when a solid induces on its surface nucleation and crystal growth of another substance or polymorph. In the pharmaceutical context, heteronucleation has been addressed by several research groups and in the review of Thakore et al. (Thakore et al., 2020) a comprehensive list of available literature can be found.

Due to the presence of impurities (dust, etc.) it is assumed that heterogeneous nucleation generally predominates over true homogeneous nucleation in real (solvent-based) crystallization processes (Liu, 2000). According to the classical nucleation theory, heterogeneous nucleation is preferred over homogeneous nucleation due to the energy barrier being lowered in the presence of a solid surface (Winter et al., 2009). In the context of particle coating this ensures nucleation and crystal growth on the solid core phase (heteroepitaxy) is being favoured over spontaneous nucleation in solution.

Several mechanisms governing heteronucleation have been proposed. The interactions occurring during heterogeneous nucleation result from either crystallographic features or surface properties of the nucleant (Thakore et al., 2020). Cross-nucleation is a particular form of heterogeneous nucleation, describing the nucleation of one polymorph on the surface of another polymorph of the same substance. It is a common mechanism, occurring both during crystallization from melt or from solution. For many substances, among them the frequently used drug excipient mannitol, the type of polymorph nucleating can be controlled, either via solvent selection or via supersaturation control (Tao et al., 2007; Yu, 2003). If polymorphic transition is absent, the cross-nucleating polymorph is required to exhibit faster crystal growth compared to the initial polymorph, in order to dominate in the final product (Yu, 2003).

Particle Engineering in Dry Powder Inhalation

The administration of dry powders to the lung to treat asthma and chronically obstructive pulmonary diseases (COPDs) is largely based on the presence of heterogeneous surface topographies (Yang et al., 2016): In order to reach the target site, active pharmaceutical ingredient (API) particles must exhibit an aerodynamic particle size of 1-5 µm. Since powders containing particles in this size range are rather cohesive and flow poorly, formulation development for dry powder inhalers (DPIs) is challenging. Developing carrier-based formulations is a common strategy to overcome this problem, resulting in formulations that are easier to handle. After blending, the small API particles adhere to the surface of a larger, free flowing, non-cohesive, carrier material (usually 50 µm – 200 µm) (Saint-Lorant et al., 2007). As the patient inhales the formulation, the release of the API from the carrier is critical for it to reach the lung. Thus, interparticle interactions play a crucial role in carrier-based formulations. They must be balanced to meet stability requirements during transport and handling of the formulation and to ensure release of the active ingredient during inhalation. The surface topography of the carrier is the target of many studies to optimize drug-carrier interactions and consequently drug release (Maas et al., 2010).

In the past, scientists have attempted to tailor the interactions between API and carrier via carrier surface modification (Scherließ et al., 2022). However, the choice of carrier has been limited to a small number of substances (mostly lactose). Besides surface topography/structure also the relevance of chemical interactions was recognized. The larger the surface area, the more API can adhere per mass of carrier particles. Hydrogen bonds and van der Waals forces between carrier and API largely depend on the contact area available, hence, large cavities present on carrier particles cause adverse effects on drug detachment (Mönckedieck et al., 2017). Up to now, the key influence factors on drug release could not be controlled independently as would be necessary to understand their individual effect on DPI performance.

Besides α-lactose, also the use of mannitol as a carrier substance has recently received a lot of attention (Hertel et al., 2020a; Kaialy et al., 2010; Pinto et al., 2021). This is related to two key advantages offered by the latter: Firstly, amino groups found in many APIs are prone to react with lactose (Maillard reaction). This unwanted effect is absent for mannitol due to its non-reducing nature. Secondly, spray-dried particles of mannitol are found to be crystalline, whereas spray-dried lactose particles are at least partly amorphous (Islam et al., 2010; Littringer et al., 2012b). Their beneficial flow behaviour results in great interest in the use of spherical spray-dried mannitol particles as a carrier material and studies have been devoted to engineering the particle's surface (Littringer et al., 2012a; Maas et al., 2010; Mönckedieck et al., 2017).

Up to now, several studies have targeted tailoring of crystalline particles suspended in a liquid phase by oscillating temperatures (i.e., temperature cycles). This approach has been shown to be particularly useful for minimization of fines content in powders with broad particle size distributions (Abu Bakar et al., 2010, 2009; Besenhard et al., 2017; Kacker et al., 2017; Kim et al., 2003; Majumder and Nagy, 2013; Wu et al., 2016), for the modification of crystal shape (Jiang et al., 2014; Lovette et al., 2011; Neugebauer et al., 2018; Snyder et al., 2007) and lately for deracemization (Breveglieri et al., 2018; Neugebauer et al., 2021). In this context tubular crystallizers offer several advantages over the corresponding processes in batch: (1) Precise control of the supersaturation, which is the key for rational control of the crystallization and the material transformation. (2) High levels of super- and under-saturation, and the ability to switch between them within seconds allows for rapid dissolution and growth, yet preventing secondary and/or primary nucleation. (3) Crystallization will occur in the absence of any moving parts and at minimum agitation, thus minimizing complexity, crystal breakage/attrition and undesired secondary nucleation (Besenhard et al., 2017).

Based on findings from earlier work on temperature cycling, in the present study an elaborate approach for coating spray-dried mannitol particles was developed. We show how cycles of crystal growth and dissolution can be used to both induce cross-nucleation of the β-polymorph and heterogeneous nucleation of a foreign substance. The deposited substance forms a coating, which can be tailored by the choice of process parameters, such as temperature gradient and pump rate.

Particles resulting from temperature cycling-induced coating were characterized in terms of surface morphology, micromeritic properties and surface energy. These analyses were complimented by investigating the performance of coated particles as carrier for a model API (salbutamol sulphate) in inhalation therapy (for an overview of our approach see Figure 1). The results show the individual influence of surface roughness and chemical properties of the coating on the attachment of API particles during blending and their detachment during inhalation.

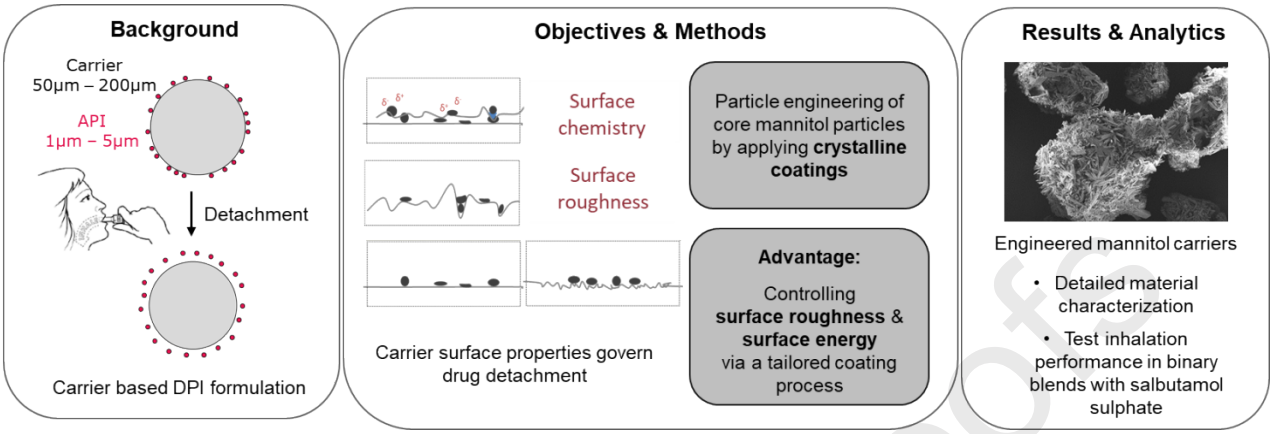

Figure 1: Overview of our approach to test particles with engineered coatings for their use in inhalation therapy.

2 MATERIALS AND METHODS

2.1 Materials

α-mannitol (Pearlitol 200SD, spray-dried form, Roquette, France), was selected as core material for crystalline coating and as a reference inhalation carrier. The coating substances urea (UR) and citric acid (CA) were purchased from Merck KGaA (Germany). Solvents (1-butanol 99.8 %, ethanol 99.8 % and acetone 99.8 %) were purchased from Carl Roth GmbH (Germany). Salbutamol sulphate (SBS) was purchased from Fagron GmbH & Co KG (Germany) and used as model drug after micronization with a 50 AS spiral-jet mill (Hosokawa, Alpine, Germany; injection pressure 8.0 bar and milling pressure 5.0 bar) to a mean particle size of 2.8 µm. β-mannitol (P160C) for inverse gas chromatography (IGC) measurements was donated from Roquette (France).

2.2 Particle Engineering – Cross-Nucleation of β-Mannitol

By now, three different polymorphic forms are known for D-mannitol, among which the β-form is most stable at ambient conditions and therefore, is the most widely used form in pharmaceutical applications. The α-polymorph is stable at dry conditions but is readily converted to the β-form when being suspended in aqueous solutions (Besenhard et al., 2017). At lower temperatures the differences in free energy between the α- and β-form decreases. Also, in solvents where mannitol generally shows lower solubility, as e.g. in ethanol, prolonged stability of the α-form was observed (Besenhard et al., 2017; Su et al., 2010)
.

Temperature cycling of α-mannitol to induce cross-nucleation of the β-polymorph on its surface was performed using a 60 % ethanol – 40 % water solution (w/w). At constant temperature (22 °C) the starting

suspension of the α-polymorph in this solvent mixture proved to be stable for several hours (Besenhard et al., 2017). For the preparation of the starting suspension the solvent was saturated with α-mannitol at 22 °C. A sieving fraction of α-mannitol between 150 – 180 µm was used as core particles in all further experiments. These particles were added to the saturated solution to a solid mass fraction of 0.8 % (w/w). By using a 4 x 0.5 cm stirrer bar at 500 rpm a uniform dispersion of the particles was achieved in a 1 L round-bottom flask, facilitating consistent withdrawal regardless of the fluid level in the flask.

Similar to investigations about crystal engineering in terms of fines content, shape, polymorphism and chirality, elaborated in three of our recent studies (Besenhard et al., 2017; Neugebauer et al., 2021, 2018) a setup for temperature cycling was applied (see Figure 2).

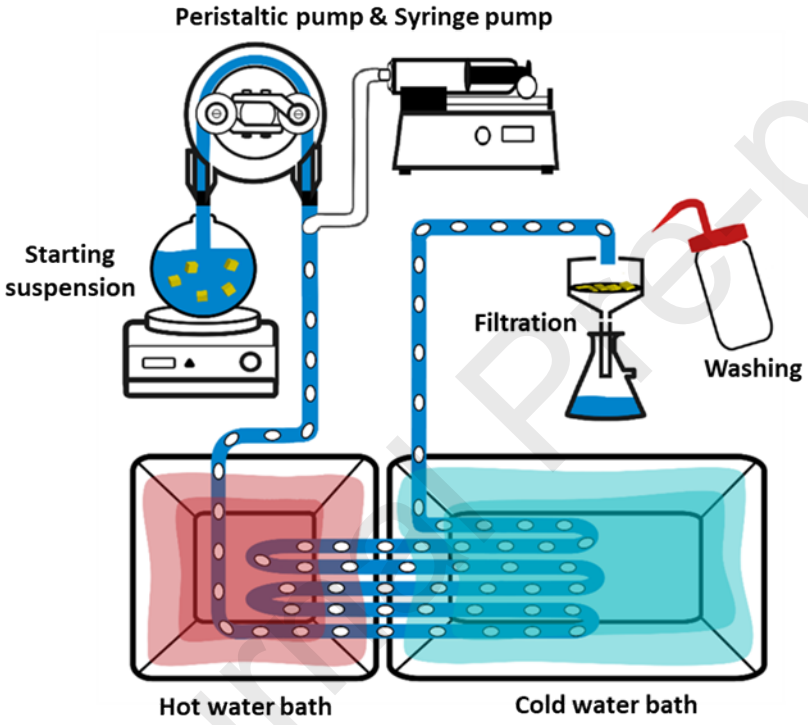

Figure 2: Schematic illustration of the temperature cycling setup, including a stirred starting suspension, a peristaltic pump and a syringe pump to facilitate segmented flow in a tubular crystallizer submerged in water baths at different temperatures (adapted from (Besenhard et al., 2017)**).**

This setup is based on polysiloxane tubing with an inner diameter d_{in} = 2 mm, alternately running through two water baths at different temperatures, one above room temperature (RT) (warm water bath) and one below (cold water bath). High heat-transfer rates realized in such tubular reactors are highly advantageous for facilitating rapid changes in supersaturation present in the cycled solution. Hence, alternating sections for nucleation/crystal growth and dissolution of coating substance could be realized. After assembly the crystallizer consisted of 25 cycles with an individual length of 1.86 m each. The distribution of tube lengths between the two water baths was unequal to account for the different rates of growth and dissolution

(110 cm of each cycle inside the cold and 55 cm inside the warm water bath and 2 × 10.5 cm for the connections in between). For each cycle the tube with an overall length of 46.5 m first passed the warm water bath, followed by the cold water bath. To overcome sedimentation effects of particles during the transit through the tube, a segmented flow was realized by continuously introducing air bubbles into the tube using a T-fitting and two syringe pumps (LA-120, HLL Landgraf, Germany). Using a peristaltic pump (Digital MS-2/6, Ismatec, USA) the mannitol suspension was pumped through the tubing at $\dot{V}_{Susp}$ = 7.2 mL/min, while the flow rate of air was 5.6 mL/min. Two different temperature settings were chosen (based on temperature-dependent solubility) in order to create particles with tailored surface coatings: T_{warm} = 27 °C and T_{cold} = 17 °C (Settings 1) and T_{warm} = 31 °C and T_{cold} = 11 °C (ettings 2). Product particles were separated from the liquid via filtration and residual water was displaced by rinsing the sample with acetone to avoid additional solvent-mediated polymorphic transition. The product particles were dried overnight in a desiccator and analyzed as detailed further below.

2.3 Particle Engineering – Heteroepitactic growth

For continuously coating mannitol particles by heteroepitactic growth we chose two pharmaceutically relevant substances to be used as coating materials: urea and citric acid. The respective choice of solvent was governed by the solubilities of the core mannitol material and the coating to be applied. The coating substance needs to exhibit a temperature-dependent solubility and the overall solubility needs to be considerable, particularly if large amounts of coating should be applied. Meanwhile, the core particles (mannitol) need to have negligible solubility. These requirements were met by using ethanol 99.8 % for urea coating and 1-butanol 99.8 % for citric acid coating.

The solvent was saturated with the respective coating substance at room temperature. In addition to that, the amount of coating substance to be deposited on the core was added to the saturated solution as ground particles for increased dissolution rate. Similar to our cross-nucleation studies, α-mannitol particles were added (150-180 µm, 0.8 % m/v) and the experiment was conducted as described in section 2.2. Respective temperature settings and the nomenclature used can be found in Table 1.

The temperature of the cold water bath (T_C) was set to room temperature, which was also the saturation temperature of the saturated solution. Thus, the amount of coating that could be deposited corresponded to the amount of solid added. The temperature of the warm water bath (T_w) was selected according to the temperature-dependent solubility of the coating substance. The higher the temperature T_w, the more coating substance was dissolved and deposited on the core particles during each cycle. However, at elevated concentrations of solute in the solution and hence higher supersaturation in the cold water bath,

increased nucleation away from the carrier particles was also observed. This was indicated by elevated numbers of free crystals of the coating substance in the product.

Table 1: Coating substances and settings used during heteroepitaxy experiments.

Coating substance	Sample name	Temperature cold water bath T_c /°C	Temperature warm water bath T_w /°C	Solubility in the solvent used		Mass fraction carrier : Solid coating substance
				at T_c	at T_w	
Mannitol	MA10	17	27	1.46 g / 100 g	2.37 g / 100 g	-
	MA20	12	32	1.16 g / 100g	2.98 g / 100 g	-
Citric acid	CA8	21	29	13.9 g / 100 g Butanol (Pascuas, 2019)	18.3 g / 100 g	3.33 : 1
	CA15	21	36		22.1 g / 100 g	3.33 : 1
Urea	UR17	21	38	5.2 g / 100 g EtOH (Lee and Lahti, 1972)	8.0 g / 100 g	3.33 : 1
	UR27	21	48		10.3 g / 100 g	3.33 : 1

2.4 Material Characterization

2.4.1 Solubility of α- and β-Mannitol in EtOH – H_2O (60/40 w/w)

The temperature dependent solubility of α- and β-mannitol in the solvent was determined using a Crystalline® device (Technobis, Netherlands). β-Mannitol was dissolved in 4 g of solvent in order to obtain concentrations between 0.8 and 5.7 g/100 g. The stirred samples were heated to 50 °C at a heating rate of 0.25 °C/min, kept at constant temperature for 10 min and, subsequently, cooled down to -12 °C (-0.25 °C/min). The cycle was repeated three times for statistical evaluation. The transmissivity of the samples was detected. Clear points and cloud points indicated the solubility and metastable zone width of the β-polymorph, respectively. For α-mannitol the solubility was determined accordingly, but performing a single heating cycle, since at the conditions tested nucleation of only the β-polymorph can be observed (Figure 3).

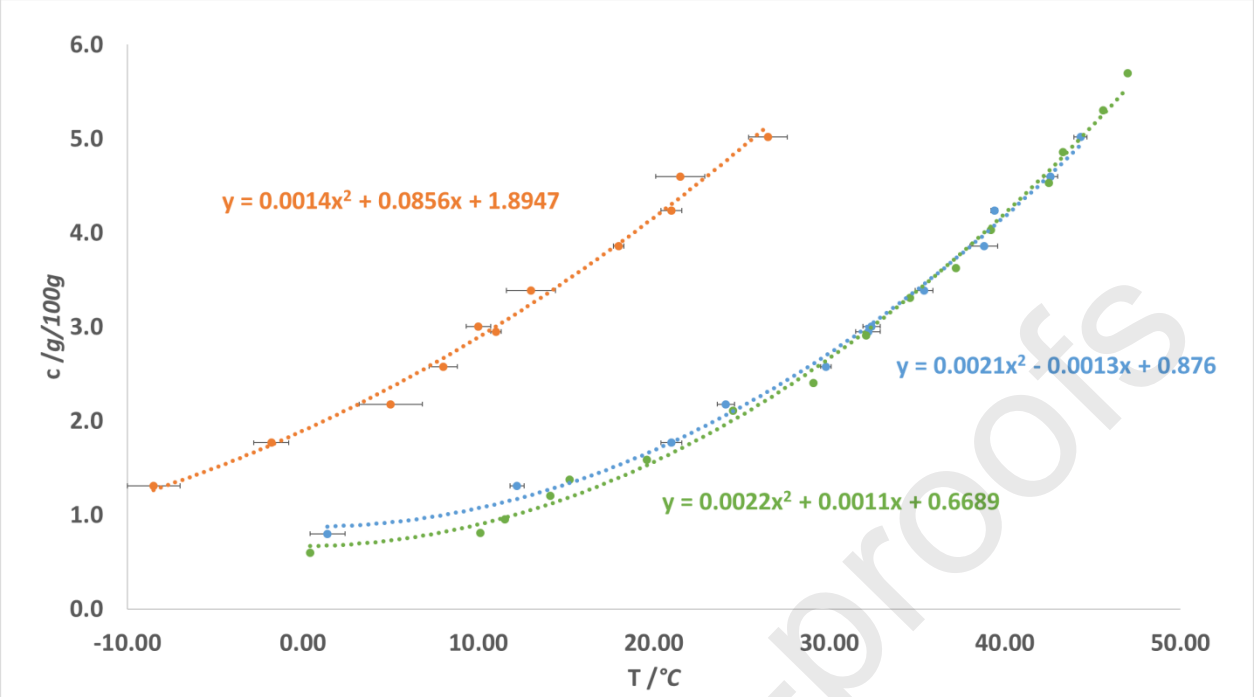

Figure 3: Solubility of α-mannitol (green) and β-mannitol (blue) in ethanol/water 60/40 (w/w) and metastable zone width of β-mannitol (orange) for a cooling rate of 0.25 °C/min. The dotted curves are representations of polynomic regressions of the data.

2.4.2 Scanning Electron Microscopy (SEM) and Roughness Determination

The surface morphology of the starting material and coated mannitol particles was observed using SEM (Zeiss Ultra 55, Zeiss, Germany). Prior to analysis all samples were gold palladium sputtered and the instrument was operated at 5 kV.

Surface roughness was determined from SEM images via Image J software. For 2 SEM images with same magnification three sections of 148 X 146 pixels (41.6 X 40.6 µm) each were selected and used to evaluate surface topography and calculate selected roughness parameters. The two statistic parameters root-mean-square roughness (Rq) and the skewness (Rsk) were selected for comparison. The Rq parameter is one of the most commonly used parameters to describe surface roughness and gives the quadratic average, or root mean square average of profile height deviations from the mean line. The Rsk parameter measures the profile symmetry about the mean line (Gadelmawla et al., 2002).

2.4.3 Raman Studies

The polymorphic composition of the samples from cross-nucleation studies was determined via Raman spectroscopy (PerkinElmer Raman Station 400, USA). Multivariate data analysis was applied to identify the ratio of mannitol's α- and β-form present by using a Partial-Least-Squares (PLS) model. Details of the

procedure, including processing of spectral data, generation and analysis of calibration sample, as well as a thorough description of the PLS model and its evaluation, are presented in one of our former publications (Besenhard et al., 2017).

2.4.4 Particle Size Characterization

The volume-based particle size distribution (PSD) of the engineered particles was investigated using laser diffraction with a HELOS system (HELOS/KR, Sympatec GmbH, Germany). A dry dispersing system (Rodos/L, Sympatec GmbH, Germany) and a vibrating chute (Vibri, Sympatec GmbH, Germany) were used for powder feeding and dispersion and a primary dispersion pressure of 0.5 bar was used. The median of the particle size distribution (x_{50}) describes a particle diameter corresponding to 50 % of the cumulative undersize of the obtained distribution. The width of the particle size distribution was expressed as span=$(x_{90}-x_{10})/x_{50}$. Measurements were made in triplicate (n=3) and data evaluation was performed using the software Windox 5.6.0.0 (Sympatec GmbH, Germany).

2.4.5 Specific Surface Area (SSA)

The SSA of the mannitol reference material as well as engineered mannitol particles was analysed (n = 2) via gas adsorption using a TriStar II 3020 system (Micromeritics, USA). Prior to analysis, samples were degassed under vacuum (VacPrep 061, Micromeritics, USA), for at least 18 hours at room temperature (22 ± 2 °C). The measurements were performed using nitrogen gas. Brunauer, Emmett, and Teller (BET) adsorption theory was used to calculate the specific surface areas, using a pressure range of 0.05–0.30 normalized to the saturation pressure of the adsorbate.

2.4.6 Particle Density

A helium pycnometer (AccuPyc II 1340, Micromeritics, USA) was used to determine the true particle volume and hence the density of engineered mannitol particles. The pycnometer used 20 purges at 19.5 psi and five analytical runs at 19.5 psi with an equilibration rate of 0.0050 psi/min. Each experiment was performed in triplicate. The density of the mannitol reference material was determined for comparison.

2.4.7 Powder X-Ray Diffraction

For mannitol samples coated with Urea, powder X-ray diffraction (PXRD) patterns were collected to proof the crystalline nature of the coating. A Siemens D5005 in Bragg-Brentano geometry equipped with a Cu-Anode (λ=1.54186A), operated at 40 kV and 40 mA was used. The measurements were performed in a 2-Theta range between 4° and 40° with a step size of 0.04° and a time per step of 2 sec (see Supplementary Information – Figure S1).

2.4.8 Determination of Surface Energy

The total surface energy, composed of dispersive (London dispersion, van der Waals, Lifshitz interactions) and specific (acid-base, polar interactions) surface energy was determined via inverse gas chromatography (Surface Energy Analyser, (IGC-SEA), Surface Measurement Systems Ltd., United Kingdom). The IGC-SEA has a unique injection mechanism which allows the precise control of the injection size, thereby precise amount (n, mole) of probe vapor can be passed through the sample column to achieve a specific probe surface coverage, n/n_m (where n_m is the monolayer adsorbed gas amount).

Samples (α- and β-mannitol, CA, UR and SBS) were packed into individual IGC-SEA silanised glass columns (inner diameter of 4 mm). Before measurement, the packed columns were pre-conditioned for 1 hour at 30 °C and 0 % RH with 10 ml/min nitrogen carrier gas. The experiment was conducted at 30 °C with 10 ml/min total flow rate of nitrogen carrier gas, and using methane for dead volume corrections. The dispersive surface energy (Ys^D) analysis was performed by measuring the net retention volume V_N (measured retention volume minus dead volume) for a series of alkane eluants (heptane, octane, nonane and decane) applying the Dorris and Gray method (Ylä-Mäihäniemi et al., 2008).

The specific surface energy (Ys^{AB}) was determined by measuring the retention volume of polar probe molecules (acetone, chloroform, ethanol, ethyl acetate, toluene and dichloromethane) on the samples applying the van Oss approach (Van Oss et al., 1988). The specific contribution is subdivided into an acid γ+ and a base γ- parameter of the surface tension. In this approach, the Della Volpe scale is employed, with a pair of mono-functional acidic and basic probe molecules (dichloromethane - γ+ : 124.58 mJ/m^2 and toluene - γ- : 16.23 mJ/m^2 (Della Volpe et al., 2004; Ho et al., 2012; Ho and Heng, 2012).

Evaluation of raw data was conducted using the IGC-SEA Analysis Software (Surface Measurement Systems Ltd., United Kingdom).

Determination of Surface Heterogeneity

Surface heterogeneity profiles can be represented by an energy distribution function and constitute an energy "map" of the material surface. Therefore, a series of probe vapours was injected at different surface coverages resulting in a distribution of surface energy as a function of surface coverage, which is referred to as a surface energy profile.

Calculation of work of adhesion and cohesion

Using the determined components for the surface energy of the solids, the work of cohesion (W_{coh}) between the API particles (SBS) and the work of adhesion (W_{adh}) between API and carrier (UR, CA, α- and β-mannitol) were calculated according to the geometric mean method:

$$Wcoh = 2[(Ys^D * Ys^D)^{\frac{1}{2}} + (Ys^+ * Ys^-)^{\frac{1}{2}} + (Ys^- * Ys^+)^{\frac{1}{2}}] \quad 1)$$

$$Wadh = 2[(Ys1^D * Ys2^D)^{\frac{1}{2}} + (Ys1^+ * Ys2^-)^{\frac{1}{2}} + (Ys1^- * Ys2^+)^{\frac{1}{2}}] \quad 2)$$

2.5 Preparation of Adhesive Mixtures

Adhesive mixtures with 2.2 % drug load (w/w) were prepared in a tumble blender TC2 (Willy A. Bachofen Maschinenfabrik, Switzerland) in closable stainless-steel vessels (inner diameter 49 mm, height 40 mm, filling volume about 40 %). The batch size was 5 g. For each mixture, the API was layered between the respective carrier using the sandwich method and blended for 60 minutes at 32 rpm. Afterwards the blend was sieved through a 400 µm sieve followed by a final mixing step of 10 minutes at 32 rpm. Additionally, prior to blending the API was sieved through a 400 µm sieve to break agglomerates (Faulhammer et al., 2015).

The homogeneity of the blends was determined by the coefficient of variation of the mean drug content (n=10 sample) obtained via a validated HPLC method (Section 2.7).

2.6 Aerodynamic Performance

The aerodynamic performance of the blends was assessed using the Next Generation Impactor (NGI) (Copley Scientific, United Kingdom) together with the Aerolizer®, a capsule-based low resistance inhaler. The mean capsule fill weight was 25 mg and 4 capsules were sequentially fired per NGI experiment. The methodology followed the European Pharmacopoeia (preparations for inhalation: aerodynamic assessment of fine particles, Ph. Eur., 7.0) and is detailed in earlier publications of our research group (Faulhammer et al., 2015; Zellnitz et al., 2017). In order to compare the performance of the engineered mannitol carriers the fine particle fraction (FPF) and the emitted fraction (EF) were chosen. The EF (%) represents the percentage of API found in the whole impactor (mouthpiece adaptor, introduction port, pre-separator, impaction stages) related to the target dose. The FPF represents the percentage of API particles exhibiting an aerodynamic diameter of < 5 µm and is one of the most common parameters to compare the performance of different DPI formulations. The FPF (%) is calculated as the ratio of fine particle mass (mass of particles below 5µm) and emitted dose (mass emitted per NGI experiment). Each blend was tested in triplicate.

2.7 High Performance Liquid Chromatography (HPLC)

SBS content was analyzed on a Waters 2695 (Waters, USA) HPLC system equipped with an autosampler and a Waters 2996 photodiode array detector (Waters, USA). The mobile phase consisted of 60 % 5 mM hexanesulfonic acid sodium salt in water +1 % acetic acid and 40% of methanol. As stationary phase a Luna® 3 µm C18 100 Å, LC column was used at a temperature of 30 °C. 50 µl of the sample were injected into the HPLC system per run and the flow rate was 1 ml/min. For the preparation of the standards, purified water adjusted to pH 3 with acetic acid was used as a diluent. Linearity was given between 2 µg/ml and 30.0 µg/ml.

3 RESULTS

3.1 Characterization of Engineered Particles

Morphology and Micromeritics

SEM images of reference mannitol and coated mannitol particles shown in Figure 4 provide evidence on how temperature cycling of particles affects the surface topography of mannitol particles. While the pristine α-mannitol particles show a comparatively smooth surface with a few needles (likely β-mannitol) scattered on it, engineered carriers exhibit crystalline structures (needles of varying sizes) distributed evenly over the surface. By changing the temperature difference (ΔT) between the two water baths the surface roughness could be manipulated. According to the SEM images and surface area measurements, employing a smaller ΔT of 10 °C resulted in a large surface area (Table 2) due to the growth of a large number of small crystallites. At higher temperature differences (ΔT 20 °C) the number of cross-nucleated crystals decreased and their individual size increased, resulting in increased surface roughness.

For heteroepitactic coating we obtained different results: For larger ΔT a larger amount of coating substance dissolves in the warm water bath, resulting in a higher supersaturation in the cold water bath. Consequently, nucleation is preferred over crystal growth and the large number of nucleation sites results in a more homogeneously covered surface.

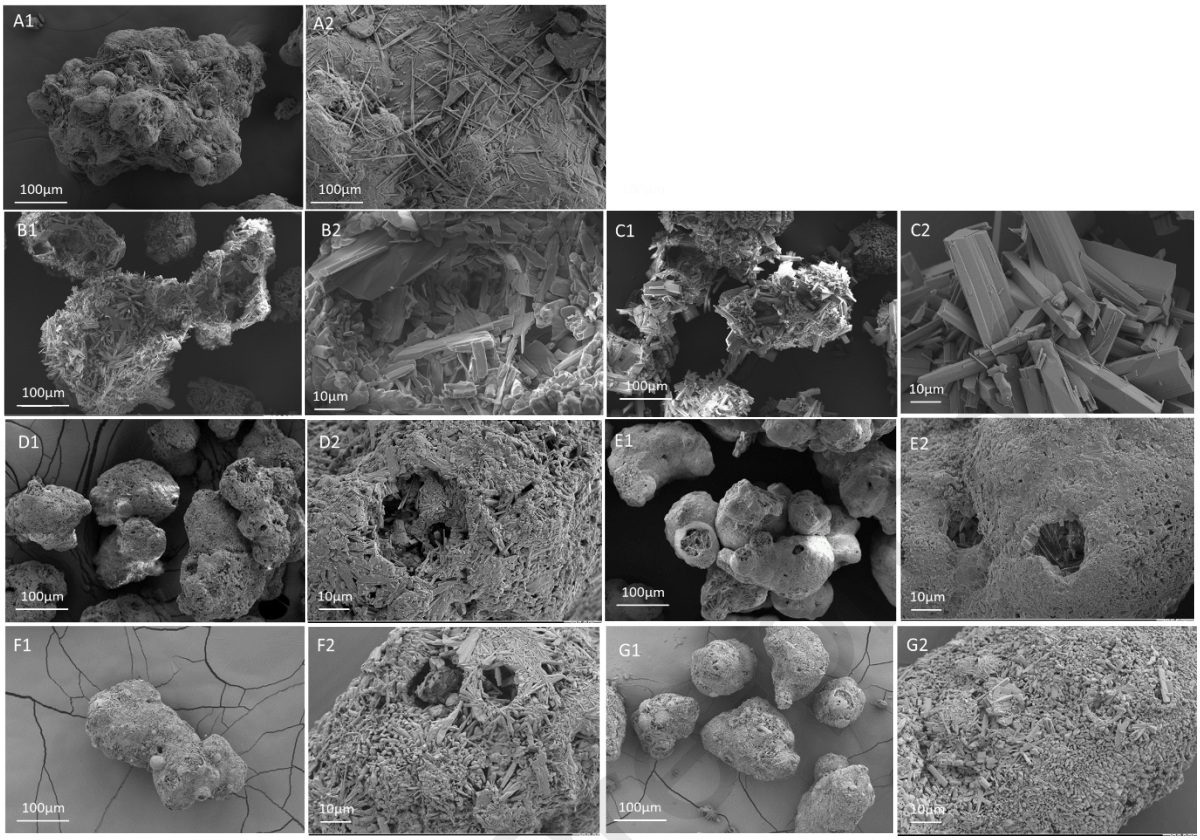

Figure 4: SEM images of A) starting material (P200SD) and engineered mannitol particles: B) MA10, C) MA20, D) CA8, E) CA15, F) UR17 and G) UR27. (1 indicated an image width of 571.6 µm and 2 and image width of 114.3 µm).

Table 2 summarizes particle characteristics of reference mannitol and engineered mannitol particles. By coating the mannitol particles, the true density changes according to the density of the respective coating substances (true density for MA = 1.52 g/cm³, CA = 1,66 g/cm³, UR = 1,32 g/cm³). The mean particle size remained unchanged for coating by cross-nucleation, which is based on dissolution and recrystallization of mannitol. For particles coated with UR and CA, though, we noticed an increase in size. Compared to the sieved reference mannitol sample the SPAN slightly increased for all engineered mannitol samples, however overall, the particle size distribution remained quite narrow (SPAN 0.92 to 1.1). Particularly for inhalation carrier materials, the presence of fine particles (< 10 µm) is an important parameter that contributes to the overall performance of the carrier (Jones and Price, 2006). Usually, a certain amount of fines (intrinsic or extrinsically added fine material, up to 10 % w/w) present in the formulation positively affects the amount of drug detached from the carrier (Zellnitz et al., 2018). Compared to the reference material, the amount of fine particles present after temperature cycling is significantly reduced for CA coated particles, followed by MA coated particles and only slightly reduced for UR coated samples.

SSA together with roughness values determined from SEM images were chosen for qualitative evaluation of the changes in surface roughness. The largest SSA was found for MA10 (large number of small mannitol

needles) followed by MA20 (fewer and thicker mannitol needles). The irregular surface structure of mannitol reference material led to an SSA in between. Compared to that, the SSA of UR coated particles is lower and that of CA coated particles even below that. This is well in accordance with observations from SEM images, revealing that the crystalline structures of CA and UR are significantly smoother compared to the product from cross-nucleation.

Compared to MA coating, for CA and UR coating the two temperature difference settings do not result in a clear difference in SSA. For UR coated particles this is also reflected in quite similar Rq and Rsk values for the two different temperature settings. Also, for CA coated particles the Rsk for both temperature settings is quite similar. But in contrast, the CA coated particles show a positive skewness (Rsk) meaning that the surface is predominantly composed of hills and UR coated particles a negative value, meaning that the surface is more composed of valleys (Gadelmawla et al., 2002). BET surface area did not reflect observations from SEM for CA coated particles but Rq values were able to discriminate; larger values were shown for CA8 showing higher surface roughness from SEM images. For MA coated particles the Rsk values were able to reflect what was observed via SEM images, the large needles on the surface of MA20 particles resulted in larger positive Rsk values compared to MA10.

The results allow us to conclude, that only the combination of several different analytical techniques leads to an accurate characterization of the particles and allows the comparison of the resulting particle characteristics among each other. Moreover, it has to be considered that differences/inconsistencies that may occur might also be related to the sample size, that is different depending on the analytical technique applied. The BET surface area for example is measured using the particle surface of hundreds of particles per measurement. By contrast, Rq and Rsk of the particles determined via Image J from SEM images, only considered selected image sections of few particles.

Table 2 Micromeritic properties of starting material and engineered particles (True density, specific surface area (SSA), mean particle size (x50), width of the PSD distribution (SPAN), amount of fines <10µm, root-mean-square roughness (Rq), skewness (Rsk) and mass fraction of mannitol's α- and β-form.

Sample	True density /(g/m³)	SSA /(m²/g)	X50 /µm	SPAN	<10 µm /%	Rq	Rsk	Mass fraction from Raman spectra and PLS model	
								α-form /%	β-form /%
Mannitol reference	1.48	2.21	172.2	0.86	1.7	33.5	0.24	99 ± 1	1 ± 1
MA10	1.48	3.33	173.3	0.96	0.9	35.8	- 0.01	86 ± 4	14 ± 4
MA20	1.48	1.67	174.1	0.97	0.7	38.1	0.15	83 ± 4	17 ± 4
CA8	1.53	0.47	185.0	1.01	0.65	48.5	0.32	-	-
CA15	1.52	0.48	184.0	0.92	0.64	29.45	0.32	-	-
UR17	1.45	0.95	188.4	0.98	1.4	37.53	-0.02	-	-
UR27	1.45	0.91	185.3	0.94	1.6	38.35	-0.01	-	-

Surface Energy

Surface energy and work of cohesion of individual components, as well as work of adhesion are essential parameters governing the performance of powders during e.g. blending processes (Begat et al., 2004) or tablet compaction and disintegration (Ramachandran et al., 2015). The same forces are underlying the operating principle of carrier-based DPI formulations. Consequently, changes in the surface energy of solids, and therefore in adhesion, are assumed to cause fundamental changes in dispersion behaviour of adhesive mixtures (Bungert et al., 2021). Therefore, surface energy as well as work of adhesion and cohesion were calculated for the materials used in the present study. Table 3 summarizes dispersive, acid-base and total surface energy at 3 different surface coverages for the reference core material (α-mannitol) as well as coating substances.

Table 3 Summary of the surface energy (SE) results of different samples at 3 different surface coverage.

Sample	Min. (SE at 0 % coverage)			γ50 (SE at 50 % coverage)			Max. (SE at 100 % coverage)		
	γS^{D} /mJ/m²	γS^{AB} /mJ/m²	γS^{TOT} /mJ/m²	γS^{D} /mJ/m²	γS^{AB} /mJ/m²	γS^{TOT} /mJ/m²	γS^{D} /mJ/m²	γS^{AB} /mJ/m²	γS^{TOT} /mJ/m²
α-mannitol (reference)	44.87	3.16	49.66	48.55	3.80	53.52	64.58	5.82	70.34
β-mannitol	38.47	3.26	42.74	40.29	6.35	44.41	48.18	7.62	51.68
CA	80.45	41.76	122.99	83.20	42.74	126.56	95.19	47.00	142.12
UR	37.91	5.93	44.04	40.41	6.27	46.86	51.31	7.75	59.11
SBS	37.00	2.98	40.66	38.64	3.55	42.23	45.76	3.69	49.01

Results show that for all samples surface energies are heterogeneously distributed over the surface, indicated by changes in surface energy as a function of surface coverage. In addition, it can clearly be observed that the dispersive component contributes significantly to the surface energy. Of all samples, the reference material (α-mannitol) shows highest surface heterogeneity, possessing surface sites with the most different levels of energy, whereas, the most homogenous surface was observed for SBS, the API applied during blending and NGI tests. CA shows the highest dispersive, specific and total surface energy, indicating that CA is more energetically active compared to the other samples. As already reported previously, the α-mannitol polymorph is energetically more active compared to the β-polymorph, indicated by higher γS^D (Cares-Pacheco et al., 2014). The values for the other samples (UR, SBS) are more or less similar to the β-mannitol polymorph.

Table 4 Work of cohesion and work of adhesion between different samples at 10% coverage.

Work of Cohesion /mJ/m²				**Work of Adhesion /mJ/m²**		**Work of Cohesion /mJ/m²**
α-mannitol	**β-mannitol**	**CA**	**UR**		**SBS**	**SBS**
108.77	87.75	250.08	89.57	**α-mannitol**	93.95	81.16
				β-mannitol	84.42	
				CA	135.89	
				UR	84.96	

The results shown in Table 4 indicate, that the work of cohesion of SBS is similar to the work of adhesion of SBS and α- mannitol, β-mannitol and UR. Only the work of adhesion between SBS and CA was significantly higher, indicating a higher tendency of SBS to adhere to CA compared to all the other materials. This leads to the assumption, that during inhalation a greater force is needed to detach the SBS particles from the CA coated carriers.

3.2 Characterization of Powder Blends

Overall, blends for inhalation therapy with a mixing homogeneity below 8% are considered homogenous (Hassan and Lau, 2010). Reference material as well as MA10, MA20 and UR27 met this criterion (Table 5). UR17 shows values slightly above and CA8 and CA15 do not form homogenous blends with the current blending procedure applied (Table 5). In DPI formulations, blending process parameters, besides drug and carrier properties, have shown to impact inhalation performance and drug detachment. In order to allow a direct comparison of all binary blends used in this study and attribute changes in inhalation performance

to the carrier properties, we kept the blending parameters constant. The poor mixing performance can be explained by the work of cohesion, that was significantly higher for CA compared to all other materials, indicating a large tendency to form agglomerates for CA. Consequently, the blending procedure likely has to be adapted to overcome the work of cohesion and break up strong CA agglomerates in order to improve mixing homogeneity.

Table 5: Mixing homogeneity (RSD of mean drug content, n=10).

Sample	Mixing Homogeneity (RSD)/%	Sample	Mixing Homogeneity (RSD)/%
Mannitol reference	2.88		
MA10	1.27	**MA20**	2.03
CA8	12.16	**CA15**	11.04
UR17	8.27	**UR27**	4.88

3.3 Aerodynamic Performance

The aerodynamic performance in terms of EF and FPF of engineered particles and reference material is summarized in Figure 5. For all samples tested the percentage of SBS delivered (EF) was above 80 %. The spray-dried reference material had an FPF value of around 43 %. For Parteck® M DPI (Merck, Germany), a commercial mannitol carrier product for DPIs FPF values in the same range (around 40 %) have been reported (Hertel et al., 2020a, 2020b). For comparison, standard tomahawk shaped lactose carriers typically show FPFs at around 20 % (blended with SBS and tested with a capsule based inhaler) (Faulhammer et al., 2018; Pinto et al., 2018).

Compared to that, the use of MA coated carrier particles exhibiting β-mannitol on their surface resulted in significantly larger values of FPF (around 60 %), however no significant difference between the two carrier types (ΔT10 and ΔT20) could be observed. Benetti et al. studied the delivery of SBS using carriers based on different mannitol polymorphs and found α- and β polymorphs to perform equally (FPF: 11 %) (Benetti et al., 2021). Polymorphs were obtained via a different technique and the resulting particles looked like an assembly of mannitol needles and the size of carrier particles was significantly smaller (23 µm). Therefore, a direct comparison is difficult as carrier particle size also largely impacts aerosolization performance. Despite great efforts in the field there is still no general agreement on how carrier particle size impacts drug detachment and what carrier size is ideal for improved performance. Most studies were performed on lactose and conflicting results are reported due to the complex interplay between carrier

and API combination, the inhalation device, the blending procedure and inhalation flow rate (Zellnitz et al., 2018).

In our approach the carrier size can be adjusted by selecting different size fractions of the core material used and can therefore be tailored to a specific inhaler type.

CA coated carriers resulting in the highest EF values resulted in lowest FPF values (2 %). This indicates strong interaction between the drug and the carrier and causes insufficient drug detachment during inhalation. This was further supported by iGC data where CA and SBS showed much higher work of adhesion compared to all other samples (see Table 4). For carriers coated with MA (carriers resulting in the highest FPF) the work of adhesion (β-mannitol and SBS) is close to the work of cohesion (SBS). An even balance between work of adhesion and work of cohesion seems to be preferential for higher drug detachment. UR coated samples showed varying FPF values, dependent on the ΔT applied during manufacturing and, hence, the surface roughness. Smaller temperature differences during temperature cycling and, consequently, larger surface roughness resulted in higher FPF values (40 %).

Results show that the detachment of drug particles from the carrier is not only governed by surface roughness, but also surface chemistry has to be considered. In the present study particles exhibiting a uniformly rough surface structure with increased SSA have shown to achieve high FPF values when there is a balance between adhesive and cohesive forces.

For the application as inhalation carriers, this study demonstrated the complex interplay of factors contributing to a high drug detachment. Both surface roughness and surface energy have shown to impact inhalation performance. The homogenously rough surfaces of coated carriers (MA10 and MA20) in combination with equal adhesive (carrier-API) and cohesive (API-API) forces within a formulation has resulted in the highest amount of SBS delivered to the lung. By contrast, greater adhesive than cohesive forces (CA8 and CA15) resulted in almost no SBS detached from the carrier and rather poor FPF values. Although, CA coated carriers showed a homogenous surface structure as well, the roughness was less pronounced and the surface area significantly reduced. UR coated particles, like MA coated particles, also exhibit a favourable balance of adhesion and cohesion forces. However, the SSA was significantly reduced and the roughness less pronounced compared to MA coated particles. This is likely the reason for the poorer inhalation performance reflected in the FPF values.

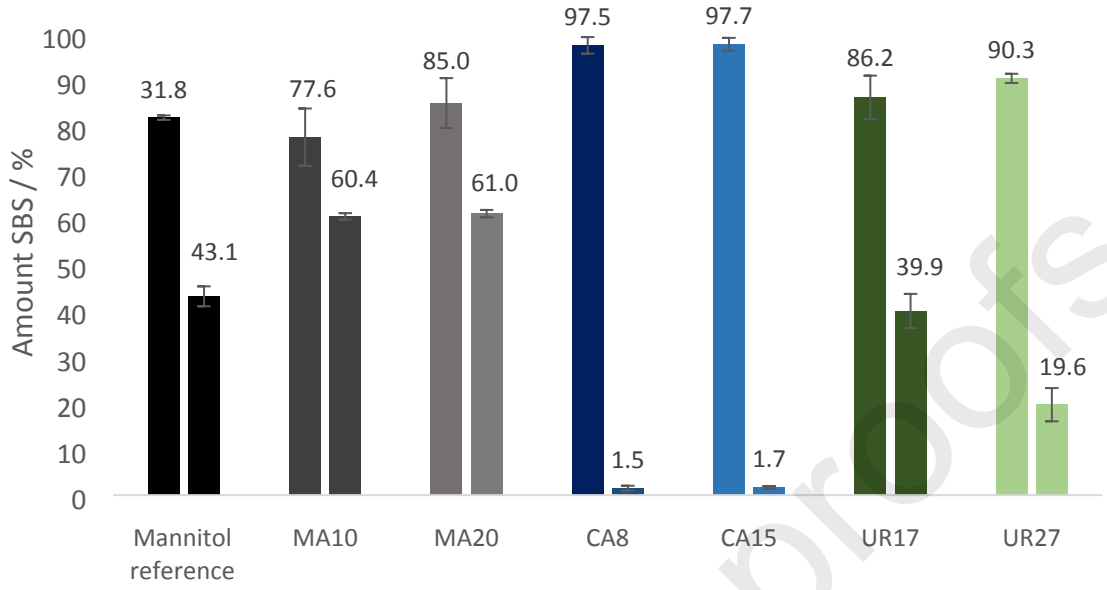

Figure 5: Percentage of SBS emitted from the inhaler (EF) (1st bar) and fine particle fraction (FPF) (2nd bar) for reference mannitol and coated carriers (mean ± SD, n=3).

4 Discussion

By now, coating processes based on crystallization from solution have only been designed for a single dissolution/re-deposition process, either in batch (Arribas Bueno et al., 2018; Mameri et al., 2017; Quon et al., 2013) or in continuous mode (Yazdanpanah et al., 2017) (see also ref (Thakore et al., 2020) for more literature on primary heterogeneous nucleation in pharmaceutical crystallization). In these set-ups tailoring the morphology of the crystalline coating is hardly feasible. Uniform coating generally depends on a slow and tightly controlled cooling rate to avoid excessive supersaturations and undesired nucleation in solution. Coating processes based on a single-step cooling crystallization often fail to result in desired surface properties if the optimal cooling trajectory is not identified. Particularly, if the amount to be deposited varies, this likely becomes a cumbersome task.

To overcome limitations imposed by batch-wise processing, we have based our concept of heteroepitactic coating on a periodic decrease in size of free crystals of the coating material and a subsequent nucleation and deposition on the core particles. Inlet and outlet temperature of the tubular crystallizer are kept at room temperature and the amount of coating substance deposited is primarily determined by the mass of solid coating material added to the saturated solution. The equilibrium solubility in the hot and cold zones and the (size-dependent) rates of crystal growth and dissolution, respectively, determine the number of cycles required.

With our approach, we not only achieve a uniform distribution of the desired amount of coating substance on the core particles, but can also tailor the surface roughness. By increasing the temperature of the warm water bath, a larger amount of coating substance dissolves per cycle, resulting in a higher supersaturation during deposition on the core particles. Our experiments on coating crystallization show, that elevated supersaturations increase the number of crystallites on the core particles' surface and decrease their individual size. Only at excessively high supersaturation spontaneous nucleation off the excipient surface resulted in less coating substance to be deposited. Similarly, incomplete (and uncontrolled) depletion of the supersaturation prior to the outlet of the tubular crystallizer has an adverse effect on the final amount of coating substance on the core particle.

Interestingly, the size of individual β-mannitol crystals after cross-nucleation was larger after cycling through a larger temperature gradient and hence higher supersaturation in the cold water bath. This might be related to the temperature of the cold water bath being altered as well.

Using spray-dried mannitol particles as core particles for applying crystalline coatings offers distinct benefits over using facetted crystals. Crystallographic matches between core particle and coating substance are relevant for heteroepitactic crystal growth on facetted crystals, likely requiring molecular modelling or induction time measurements to identify feasible combinations (Chadwick et al., 2012). In contrast, spray-dried particles display micro- and nano-sized pores, offering a large number of local spots with low effective energy barriers for nucleation (Mameri et al., 2017; Thakore et al., 2020). Also, due to their free-flowing properties, defined size fraction of particles to be coated can simply be sieved from the commercial product and powder dosing is straightforward.

The coated particles resulting from temperature cycling showed a uniform distribution of small surface crystals, which are less likely to break off during downstream processing. Provided that a solvent is identified which does not dissolve the core particles, substances (including APIs) showing temperature-dependent solubility can be selected for coating. Since only the coating substance is in solution, the potential formation of co-crystals is avoided. With targeted selection of the coating substance and temperature gradient, the physical and chemical parameters of the particle surface can be changed in directed manner. This is particularly interesting if inter-particle forces such as cohesion and adhesion are to be tailored.

In conclusion, for the application as carrier particles in DPIs, carriers with a homogenous rough surface area and increased SSA in combination with an overall low surface energy and an equal balance of adhesive and cohesive forces within the formulation have led to the most homogenous blends and the best aerosolization performance. MA coated mannitol particles served all these criteria and showed FPF values of SBS significantly higher compared to previously reported mannitol carriers.

Coating crystallization offers the advantage of introducing tailored surface roughness, needed to control interparticle forces and drug detachment. On the other hand, coating crystallization allows to simultaneously adapt surface chemistry by choosing the coating agent based on surface energy considerations. Based on surface energy data from iGC, the coating agent can be selected in order to tailor the performance of selected/given formulations (APIs) for inhalation therapy.

5 Conclusion

The development of a method to coat particles by either a cross-nucleation- or a heterogeneous nucleation-based mechanism could be highly relevant for several different (pharmaceutical) areas. The surface of particles is where they interact with the environment and therefore represents the target for a variety of engineering approaches. To demonstrate the feasibility and benefits of our approach, for the present work we have taken an example from pharmaceutical development, in which particle-particle interaction plays a particularly important role. In inhalation therapy the interaction of carrier particles with each other determines their behaviour during storage and dosing. During loading of the carrier particles with respirable, micronized API particles the complexity is even increased by introducing another chemical entity. Adhesion of the API during mixing and its detachment during inhalation present intricate challenges to formulation developers. Frequently, fines of the carrier substance need to be added to the mixture in order to saturate “hotspots” on the carrier surface and control the different adhesive forces that occur (Grasmeijer et al., 2014; Hertel et al., 2020a).

A much more straightforward approach to tackle this issue can be found in tailoring surface properties during formation of crystalline coatings, as we show in the present study. While the number of different amorphous coatings available is limited, a process for depositing crystalline materials allows to choose from a much larger number of candidate substances. This enables fine-tuning of the chemical parameters of the carrier particles’ surface regarding its polarity, surface energy and exhibition of functional groups to develop intermolecular interactions (dispersion forces and electrostatic forces).

In this study we demonstrate temperature cycling-induced formation of coatings (based on either cross-nucleation or heteroepitactic growth), to result in particles with desired changes in surface properties.

In contrast to the starting material, the engineered particles show a uniform surface topography, which is essential for controlling and tailoring interparticle interactions, e.g. in inhalation therapy. We showed how different temperature gradients are able to generate on-demand surface roughness. While for other particle engineering techniques manipulation of surface topography is usually linked to changes in particle size and/or shape, this is not the case for our setup. Therefore, we were able to selectively investigate the impact of particle surface roughness on drug detachment and inhalation performance. A future application

of our approach will be the use in depositing defined amounts of API on excipients, eliminating the need for cumbersome process steps during dosage form manufacturing (e.g. dosing, blending, granulation, etc.)

Funding

The Research Center Pharmaceutical Engineering (RCPE) is funded within the framework of COMET - Competence Centers for Excellent Technologies by BMK, BMDW, Land Steiermark, and SFG. The COMET program is managed by the FFG.

References

Abu Bakar, M.R., Nagy, Z.K., Rielly, C.D., 2010. Investigation of the Effect of Temperature Cycling on Surface Features of Sulfathiazole Crystals during Seeded Batch Cooling Crystallization. Cryst. Growth Des. 10, 3892–3900. https://doi.org/10.1021/cg1002379

Abu Bakar, M.R., Nagy, Z.K., Rielly, C.D., 2009. Seeded Batch Cooling Crystallization with Temperature Cycling for the Control of Size Uniformity and Polymorphic Purity of Sulfathiazole Crystals. Org. Process Res. Dev. 13, 1343–1356. https://doi.org/10.1021/op900174b

Arribas Bueno, R., Crowley, C.M., Davern, P., Hodnett, B.K., Hudson, S., 2018. Heterogeneous Crystallization of Fenofibrate onto Pharmaceutical Excipients. Cryst. Growth Des. 18, 2151–2164. https://doi.org/10.1021/acs.cgd.7b01598

Begat, P., Morton, D.A. V, Staniforth, J.N., Price, R., 2004. The cohesive-adhesive balances in dry powder inhaler formulations II: Influence on fine particle delivery characteristics. Pharm. Res. 21, 1826–1833. https://doi.org/10.1023/B:PHAM.0000045236.60029.cb

Benetti, A.A., Bianchera, A., Buttini, F., Bertocchi, L., Bettini, R., 2021. Mannitol polymorphs as carrier in dpis formulations: Isolation characterization and performance. Pharmaceutics 13, 1–21. https://doi.org/10.3390/pharmaceutics13081113

Besenhard, M.O., Neugebauer, P., Scheibelhofer, O., Khinast, J.G., 2017. Crystal Engineering in Continuous Plug-Flow Crystallizers. Cryst. Growth Des. 17, 6432–6444. https://doi.org/10.1021/acs.cgd.7b01096

Breveglieri, F., Maggioni, G.M., Mazzotti, M., 2018. Deracemization of NMPA via Temperature Cycles. Cryst. Growth Des. 18, 1873–1881. https://doi.org/10.1021/acs.cgd.7b01746

Bungert, N., Kobler, M., Scherließ, R., 2021. Surface energy considerations in ternary powder blends for inhalation. Int. J. Pharm. 609. https://doi.org/10.1016/j.ijpharm.2021.121189

Cares-Pacheco, M.G., Vaca-Medina, G., Calvet, R., Espitalier, F., Letourneau, J.-J., Rouilly, a, Rodier, E., 2014. Physicochemical characterization of d-mannitol polymorphs: The challenging surface energy determination by inverse gas chromatography in the infinite dilution region. Int. J. Pharm. 475, 69–81. https://doi.org/10.1016/j.ijpharm.2014.08.029

Chadwick, K., Chen, J., Myerson, A.S., Trout, B.L., 2012. Toward the rational design of crystalline surfaces for heteroepitaxy: Role of molecular functionality. Cryst. Growth Des. 12, 1159–1166. https://doi.org/10.1021/cg2010858

Della Volpe, C., Maniglio, D., Brugnara, M., Siboni, S., Morra, M., 2004. The solid surface free energy calculation: I. In defense of the multicomponent approach. J. Colloid Interface Sci. 271, 434–453. https://doi.org/10.1016/j.jcis.2003.09.049

Faulhammer, E., Wahl, V., Zellnitz, S., Khinast, J.G., Paudel, A., 2015. Carrier-based dry powder inhalation: Impact of carrier modification on capsule filling processability and in vitro aerodynamic performance.

Int. J. Pharm. 491, 231–242. https://doi.org/10.1016/j.ijpharm.2015.06.044

Faulhammer, E., Zellnitz, S., Wutscher, T., Stranzinger, S., Zimmer, A., Paudel, A., 2018. Performance indicators for carrier-based DPIs: Carrier surface properties for capsule filling and API properties for in vitro aerosolisation. Int. J. Pharm. 536, 326–335. https://doi.org/10.1016/j.ijpharm.2017.12.004

Gadelmawla, E.S., Koura, M.M., Maksoud, T.M.A., Elewa, I.M., Soliman, H.H., 2002. Roughness parameters. J. Mater. Process. Technol. 123, 133–145. https://doi.org/10.1016/S0924-0136(02)00060-2

Gaur, P.K., Mishra, S., Gautam, R., Singh, A.P., Yasir, M., 2014. Film Coating Technology: Past, Present and Future. J. Pharm. Sci. Pharmacol. 1, 57–67. https://doi.org/10.1166/jpsp.2014.1007

Grasmeijer, F., Lexmond, A.J., van Den Noort, M., Hagedoorn, P., Hickey, A.J., Frijlink, H.W., de Boer, A.H., 2014. New mechanisms to explain the effects of added lactose fines on the dispersion performance of adhesive mixtures for inhalation. PLoS One 9. https://doi.org/10.1371/journal.pone.0087825

Hassan, M.S., Lau, R., 2010. Inhalation performance of pollen-shape carrier in dry powder formulation with different drug mixing ratios: comparison with lactose carrier. Int. J. Pharm. 386, 6–14. https://doi.org/10.1016/j.ijpharm.2009.10.047

Hertel, N., Birk, G., Scherließ, R., 2020a. Performance tuning of particle engineered mannitol in dry powder inhalation formulations. Int. J. Pharm. 586, 119592. https://doi.org/10.1016/j.ijpharm.2020.119592

Hertel, N., Birk, G., Scherließ, R., 2020b. Particle engineered mannitol for carrier-based inhalation – A serious alternative? Int. J. Pharm. 577, 118901. https://doi.org/10.1016/j.ijpharm.2019.118901

Ho, R., Heng, J.Y.Y., 2012. A review of inverse gas chromatography and its development as a tool to characterize anisotropic surface properties of pharmaceutical solids. KONA Powder Part. J. 30, 164–180. https://doi.org/10.14356/kona.2013016

Ho, R., Naderi, M., Heng, J.Y.Y., Williams, D.R., Thielmann, F., Bouza, P., Keith, A.R., Thiele, G., Burnett, D.J., 2012. Effect of milling on particle shape and surface energy heterogeneity of needle-Shaped crystals. Pharm. Res. 29, 2806–2816. https://doi.org/10.1007/s11095-012-0842-1

Islam, M.I.U., Sherrell, R., Langrish, T.A.G., 2010. An investigation of the relationship between glass transition temperatures and the crystallinity of spray-dried powders. Dry. Technol. 28, 361–368. https://doi.org/10.1080/07373931003641586

Jiang, M., Zhu, X., Molaro, M.C., Rasche, M.L., Zhang, H., Chadwick, K., Raimondo, D.M., Kim, K.K.K., Zhou, L., Zhu, Z., Wong, M.H., O'Grady, D., Hebrault, D., Tedesco, J., Braatz, R.D., 2014. Modification of Crystal Shape through Deep Temperature Cycling. Ind. Eng. Chem. Res. 53, 5325–5336. https://doi.org/10.1021/ie400859d

Jones, M.D., Price, R., 2006. The influence of fine excipient particles on the performance of carrier-based dry powder inhalation formulations. Pharm. Res. 23, 1665–74. https://doi.org/10.1007/s11095-006-9012-7

Kacker, R., Radoiu, M., Kramer, H.J.M., 2017. Novel design integrating a microwave applicator into a crystallizer for rapid temperature cycling . A direct nucleation control study. https://doi.org/10.1021/acs.cgd.7b00368

Kaialy, W., Momin, M.N., Ticehurst, M.D., Murphy, J., Nokhodchi, A., 2010. Engineered mannitol as an alternative carrier to enhance deep lung penetration of salbutamol sulphate from dry powder inhaler. Colloids Surf. B. Biointerfaces 79, 345–56. https://doi.org/10.1016/j.colsurfb.2010.04.016

Kim, J.W., Ulrich, J., 2003a. Coating of Pastilles by Crystallization. Chemie Ing. Tech. 719–724.

Kim, J.W., Ulrich, J., 2003b. Development of a New Coating process in Pharmaceutical Industry by Crystallization. Eng. Life Sci. 3, 121–126. https://doi.org/10.1002/elsc.200390014

Kim, S., Wei, C., Kiang, S., 2003. Crystallization Process Development of an Active Pharmaceutical Ingredient and Particle Engineering via the Use of Ultrasonics and Temperature Cycling. Org. Process Res. Dev. 7, 997–1001. https://doi.org/10.1021/op034107t

Lee, F.M., Lahti, L.E., 1972. Solubility of Urea in Water-Alcohol Mixtures. J. Chem. Eng. Data 17, 304–306. https://doi.org/10.1021/je60054a020

Littringer, E.M., Mescher, A., Eckhard, S., Schröttner, H., Langes, C., Fries, M., Griesser, U., Walzel, P., Urbanetz, N.A., 2012a. Spray drying of Mannitol as a drug carrier—the impact of process parameters on product properties. Dry. Technol. 30, 114–124. https://doi.org/10.1080/07373937.2011.620726

Littringer, E.M., Mescher, A., Schroettner, H., Achelis, L., Walzel, P., Urbanetz, N.A., 2012b. Spray dried mannitol carrier particles with tailored surface properties - The influence of carrier surface roughness and shape. Eur. J. Pharm. Biopharm. 82, 194–204. https://doi.org/10.1016/j.ejpb.2012.05.001

Liu, X.Y., 2000. Heterogeneous nucleation or homogeneous nucleation? J. Chem. Phys. 112, 9949–9955. https://doi.org/10.1063/1.481644

Lovette, M.A., Muratore, M., Doherty, M.F., 2011. Crystal Shape Modification Through Cycles of Dissolution and Growth: Attainable Regions and Experimental Validation. AIChE J. 58, 1465–1474. https://doi.org/10.1002/aic

Maas, S.G., Schaldach, G., Walzel, P.E., Urbanetz, N.A., 2010. Tailoring dry powder inhaler performance by modifying carrier surface topography by spray drying. At. Sprays 20, 763–774. https://doi.org/10.1615/AtomizSpr.v20.i9.20

Majumder, A., Nagy, Z.K., 2013. Fines Removal in a Continuous Plug Flow Crystallizer by Optimal Spatial Temperature Profiles with Controlled Dissolution. AIChE J. 59, 4582–4594. https://doi.org/10.1002/aic

Mameri, F., Koutchoukali, O., Bouhelassa, M., Hartwig, A., Nemdili, L., Ulrich, J., 2017. The feasibility of coating by cooling crystallization on ibuprofen naked tablets. Front. Chem. Sci. Eng. 11, 211–219. https://doi.org/10.1007/s11705-017-1619-1

Mönckedieck, M., Kamplade, J., Fakner, P., Urbanetz, N.A., Walzel, P., Steckel, H., Scherließ, R., 2017. Dry powder inhaler performance of spray dried mannitol with tailored surface morphologies as carrier and salbutamol sulphate. Int. J. Pharm. 524, 351–363. https://doi.org/10.1016/j.ijpharm.2017.03.055

Neugebauer, P., Cardona, J., Besenhard, M.O., Peter, A., Gruber-Woelfler, H., Tachtatzis, C., Cleary, A., Andonovic, I., Sefcik, J., Khinast, J.G., 2018. Crystal Shape Modification via Cycles of Growth and Dissolution in a Tubular Crystallizer. Cryst. Growth Des. 18, 4403–4415. https://doi.org/10.1021/acs.cgd.8b00371

Neugebauer, P., Triebl, A., Gruber-Woelfler, H., 2021. Complete chiral resolution in a continuous flow crystallizer with recycle stream. J. Flow Chem. 11, 483–493. https://doi.org/10.1007/s41981-021-00173-2

Pascuas, O.M.O., 2019. Evaluaciòn de la Producciòn de Trietil Citrato y Tributil Citrato a Partir de la Esterificaiòn Àcida del Àcido Citrico con Etanol y 1-Butanol. Universidad Nacional De Colombia.

Pinto, J.T., Zellnitz, S., Guidi, T., Roblegg, E., Paudel, A., 2018. Assessment of Dry Powder Inhaler Carrier Targeted Design: A Comparative Case Study of Diverse Anomeric Compositions and Physical Properties of Lactose. Mol. Pharm. 15, 2827–2839. https://doi.org/10.1021/acs.molpharmaceut.8b00333

Pinto, J.T., Zellnitz, S., Guidi, T., Schiaretti, F., Schroettner, H., 2021. Spray-Congealing and Wet-Sieving as Alternative Processes for Engineering of Inhalation Carrier Particles : Comparison of Surface Properties , Blending and In Vitro Performance. Pharm. Res.

Quon, J.L., Chadwick, K., Wood, G.P.F., Sheu, I., Brettmann, B.K., Myerson, A.S., Trout, B.L., 2013. Templated nucleation of acetaminophen on spherical excipient agglomerates. Langmuir 29, 3292–3300. https://doi.org/10.1021/la3041083

Ramachandran, V., Murnane, D., Hammond, R.B., Pickering, J., Roberts, K.J., Soufian, M., Forbes, B., Jaffari, S., Martin, G.P., Collins, E., Pencheva, K., 2015. Formulation pre-screening of inhalation powders using computational atom-atom systematic search method. Mol. Pharm. 12, 18–33. https://doi.org/10.1021/mp500335w

Römbach, E., Ulrich, J., 2007. Self-controlled coating process for drugs. Cryst. Growth Des. 7, 1618–1622. https://doi.org/10.1021/cg070071a

Saint-Lorant, G., Leterme, P., Gayot, A., Flament, M.P., 2007. Influence of carrier on the performance of dry powder inhalers. Int. J. Pharm. 334, 85–91. https://doi.org/10.1016/j.ijpharm.2006.10.028

Scherließ, R., Bock, S., Bungert, N., Neustock, A., Valentin, L., 2022. Particle engineering in dry powders for inhalation. Eur. J. Pharm. Sci. 172. https://doi.org/10.1016/j.ejps.2022.106158

Snyder, R.C., Studener, S., Doherty, M.F., 2007. Manipulation of Crystal Shape by Cycles of Growth and Dissolution. AIChE J. 53, 1510–1517. https://doi.org/10.1002/aic

Su, W., Hao, H., Barrett, M., Glennon, B., 2010. The impact of operating parameters on the polymorphic transformation of D-Mannitol characerized in situ with Raman spectroscopy, FBRM, and PVM. Org. Process Res. Dev. 14, 1432–1437.

Tao, J., Jones, K.J., Yu, L., 2007. Cross-Nucleation between D -Mannitol Polymorphs in Seeded Crystallization. Cryst. Growth Des. 7, 2410–2414. https://doi.org/10.1021/cg070387i

Thakore, S.D., Sood, A., Bansal, A.K., 2020. Emerging role of primary heterogeneous nucleation in pharmaceutical crystallization. Drug Dev. Res. 81, 3–22. https://doi.org/10.1002/ddr.21622

Van Oss, C.J., Chaudhury, M.K., Good, R.J., 1988. Interfacial Lifshitz-van der Waals and polar interactions in macroscopic systems. Chem. Rev. 88, 927–941. https://doi.org/10.1021/cr00088a006

Winter, D., Virnau, P., Binder, K., 2009. Monte carlo test of the classical theory for heterogeneous nucleation barriers. Phys. Rev. Lett. 103, 1–4. https://doi.org/10.1103/PhysRevLett.103.225703

Wu, Z., Yang, S., Wu, W., 2016. Application of temperature cycling for crystal quality control during crystallization. CrystEngComm 18, 2222–2238. https://doi.org/10.1039/C5CE02522B

Yang, M.Y., Verschuer, J., Shi, Y., Song, Y., Katsifis, A., Eberl, S., Wong, K., Brannan, J.D., Cai, W., Finlay, W.H., Chan, H.-K., 2016. The effect of device resistance and inhalation flow rate on the lung deposition of orally inhaled mannitol dry powder. Int. J. Pharm. 513, 294–301. https://doi.org/10.1016/j.ijpharm.2016.09.047

Yazdanpanah, N., Testa, C.J., Perala, S.R.K., Jensen, K.D., Braatz, R.D., Myerson, A.S., Trout, B.L., 2017. Continuous Heterogeneous Crystallization on Excipient Surfaces. Cryst. Growth Des. 17, 3321–3330. https://doi.org/10.1021/acs.cgd.7b00297

Ylä-Mäihäniemi, P.P., Heng, J.Y.Y., Thielmann, F., Williams, D.R., 2008. Inverse gas chromatographic method for measuring the dispersive surface energy distribution for particulates. Langmuir 24, 9551–9557. https://doi.org/10.1021/la801676n

Yu, L., 2003. Nucleation of one polymorph by another. J. Am. Chem. Soc. 125, 6380–6381. https://doi.org/10.1021/ja0351544

Zellnitz, S., Roblegg, E., Pinto, J., Fröhlich, E., 2018. Delivery of dry powders to the lungs : Influence of particle attributes from a biological and technological point of view 1. https://doi.org/10.2174/1567201815666181024143249

Zellnitz, S., Zellnitz, L., Roblegg, E., Fröhlich, E., 2017. Impact of Salbutamol Sulphate Particle Properties on Biological Effects in the Lung Sarah, in: Drug Delivery to the Lung 28. pp. 274–277.

Sarah Zellnitz: Conceptualization, Methodology, Formal Analysis, Writing – Original Draft, Writing – Review & Editing; **Magdalena Lanzinger**: Investigation; **Hartmuth Schroettner**: Resources, Investigation; **Majid Naderi**: Resources, Investigation; **Meishan Guo**: Resources, Investigation; **Amrit Paudel**: Resources; **Heidrun Gruber-Woelfler**: Conceptualization, Supervision; **Peter Neugebauer**: Conceptualization, Methodology, Writing – Original Draft, Writing – Review & Editing, Supervision, Project Administration,

Declaration of interests

☐ The authors declare that they have no known competing financial interests or personal relationships that could have appeared to influence the work reported in this paper.

☒ The authors declare the following financial interests/personal relationships which may be considered as potential competing interests:

Peter Neugebauer reports financial support was provided by Die Österreichische Forschungsförderungsgesellschaft FFG.